# Design Implications of Rotordynamics and Mass Balancing on a 1.4 MW Partially Superconducting Machine

Kirsten P. Duffy[1]
*University of Toledo, Toledo, OH, 43606, USA*

Justin J. Scheidler[2]
*NASA Glenn Research Center, Cleveland, OH, 44135, USA*

**To ensure that rotating machines operate without excessive bearing loads, vibration, and dynamic stresses, their design must consider rotordynamic response and provisions for mass balancing of rotors, even when their rotational speeds are modest. This paper presents a rotordynamics design study for a 1.4 MW, partially superconducting electric machine proposed for electrified aircraft propulsion – NASA's High Efficiency Megawatt Motor (HEMM). The study includes the selection of mass balancing grade and mount and bearing stiffnesses to yield satisfactory critical speeds, deflection, and unbalance force, and predictions of the expected mass unbalance caused by the superconducting rotor coils. The impact of the machine's number of rotor poles on expected mass unbalance is also quantified. Design decisions and lessons learned are discussed.**

## I. Introduction

Aircraft with electrified propulsion systems require electric machines that are very lightweight and highly efficient. Advancements to the state of the art are needed to meet this demand. This is particularly true for large transport aircraft with more than about 150 passengers, which will require electric machines with power ratings in the 1 to 30+ MW range. At this scale of power, superconducting technology becomes attractive for electrified aircraft propulsion to increase efficiency and reduce mass [1]. A mass reduction relative to non-superconducting machines can result from an increase in the specific power of the machine and indirectly through a significant reduction in the amount of waste heat generated on the aircraft, which reduces the mass of the thermal management system [2]. NASA's High Efficiency Megawatt Motor (HEMM) is a 1.4 MW partially superconducting machine that is being developed to achieve an efficiency greater than 98% and electromagnetic specific power greater than 16 kW/kg. The HEMM contains a copper stator operating above room temperature and a superconducting rotor composed of no-insulation 2nd generation high temperature superconducting (HTS) coils that operate below 62 K (-211 °C). The superconducting coils are conductively cooled by a pulse tube cryocooler embedded inside and rotating with the rotor shaft. This paper presents a rotordynamics study for the HEMM, including the selection of mass balancing grade and mount and bearing stiffness to yield satisfactory critical speeds, deflections, and unbalance forces. The unbalance generated by the superconducting coils arises mainly due to manufacturing variability and can be minimized through targeted distribution of coils around the rotor. The rotor is overhung, which complicates the mount structure design in order to place critical speeds outside the operating speed range and to damp vibrations occurring when running through those critical speeds. Mount structure designs are discussed, and results for unbalance response are given.

[1] Senior Research Associate, Mechanical, Industrial and Manufacturing Engineering Department, AIAA Member.
[2] Research Aerospace Technologist, Rotating and Drive Systems Branch, Materials and Structures Division.

## II. Overview of the HEMM and its Superconducting Rotor

The HEMM is sized to satisfy the requirements of each generator of the Single-Aisle Turboelectric Aircraft with Aft Boundary Layer (STARC–ABL) concept [3]. The key performance parameters of the HEMM – an efficiency >98% and a specific power of >16 kW/kg relative to electromagnetic weight – can enable meaningful reductions in the fuel burn of this concept aircraft [2]. The machine is designed to produce 2 kNm of torque at a speed of 6,800 rpm. This is achieved using a rotor tip speed of only 107 m/s (Mach 0.31). The main subassemblies of the HEMM are depicted in Fig. 1. The stator employs a copper armature winding that is oil cooled and operates an average temperature around 423 K (150 °C) [4]. The field windings on the rotor are composed of 2nd generation high temperature superconducting (HTS) coils that operate below 62 K (-211 °C) [5-7]. The rotor is conductively cooled using a rotating, Stirling-type, pulse tube cryocooler that is integrated inside the machine's shaft [8-9]. Hence, the HEMM is a cryogen-free machine that appears to be non-superconducting from the perspective of the aircraft.

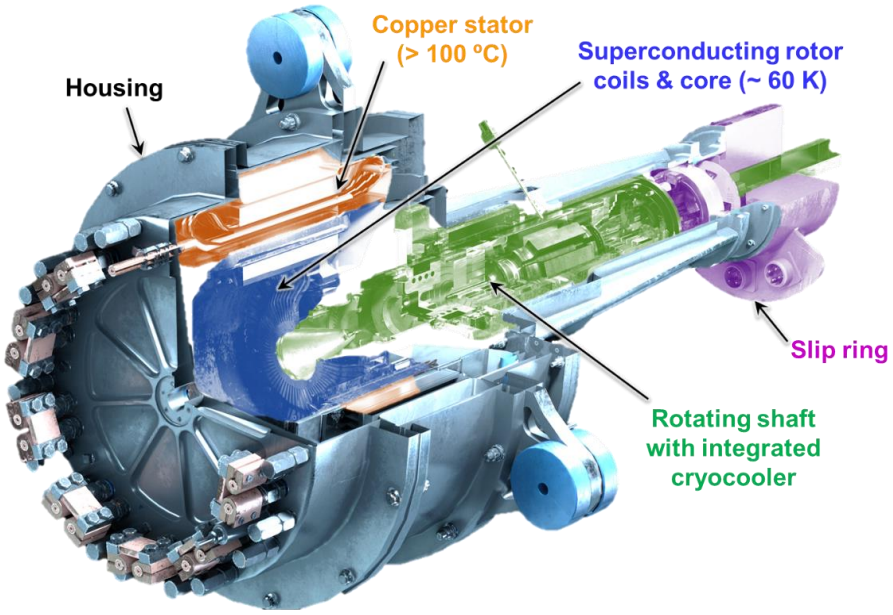


**Fig. 1 Subassemblies of NASA's high efficiency megawatt motor (HEMM).**

Figure 2 depicts the superconducting rotor in more detail. The rotor contains 12 poles, which results in a fundamental electrical frequency of 680 Hz. Each pole is a no-insulation quadruple racetrack coil that nominally contains 600 turns of HTS (i.e., 150 turns per racetrack). The racetrack coils in each pole are electrically connected using HTS jumpers. A vacuum tube surrounds the rotor core, with the wall located between the stator coils and the rotor coils.

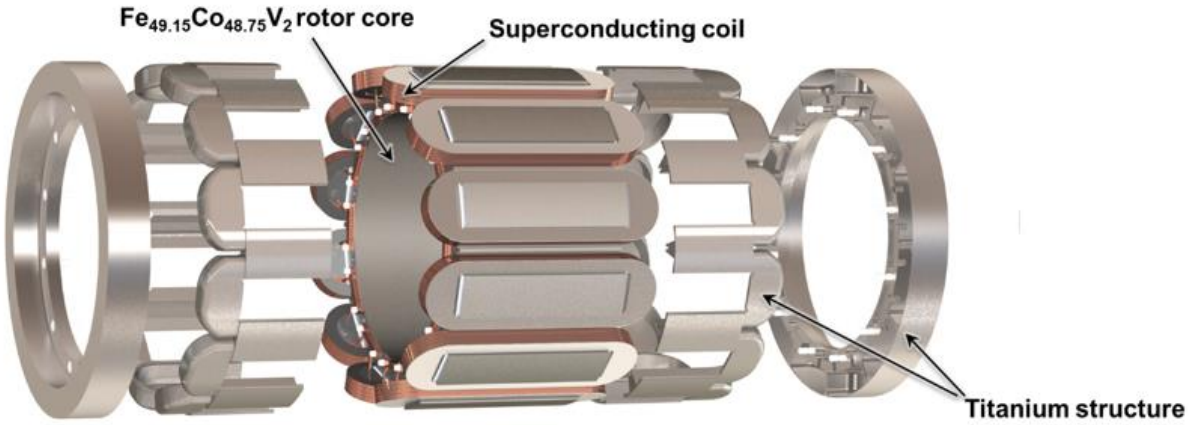


**Fig. 2 Exploded view of the HEMM's superconducting rotor.**

## III. Mass Balancing of a Superconducting Rotor

In most superconducting rotors, the dominant mass unbalance is expected to arise from the superconducting coils due to the density of HTS and copper, their imprecise winding from long lengths of conductor, and their assembled construction. Machined, stamped, and laser cut structural and magnetic parts will introduce unbalance, but the magnitude can be more readily controlled through tolerancing and symmetric design. The unbalance caused by superconducting coils is also more difficult to correct, because the coils are purposefully located near the outer diameter of the rotor and mass corrections likely cannot be made to the coils themselves. Also, it is important to anticipate the mass unbalance that will occur before a design is finalized to ensure adequate material or features are available for enacting corrections. Consequently, this paper introduces a method to predict and minimize the mass unbalance caused by superconducting rotor coils.

The first step in predicting the unbalance caused by the superconducting rotor coils is to quantify the variability in the geometry of each HTS racetrack coil layer that composes each rotor coil. The winding fixture used to fabricate the HEMM's racetrack coil layers is depicted in Fig. 3. A conventional tolerance stack-up analysis of the winding assembly was conducted to define the envelope geometry of each racetrack coil layer, as shown in Fig. 4, due to a worst case stack up of the dimensions and tolerances on each part. This information was used along with the manufacturer's tolerance on the superconductor to quantify the expected number of turns in each racetrack coil layer. Note that the HEMM coils are wound to a defined size not a fixed number of turns. The expected number of turns per racetrack coil layer is 167 turns with a tolerance of -19 / +18 turns. This large tolerance was found to be primarily caused by the tolerance on the conductor's thickness. The tolerances of the machined winding fixture led to a tolerance of -3 / +0 turns, whereas the conductor's thickness tolerance contributes the remaining -16 / +18 turns. Hence, manufacturing improvements to the superconductor are the only factor that can appreciably reduce the tolerance on number of turns.

**Fig. 3 Winding fixture used to manufacture the full-scale HTS racetrack coil layers for the HEMM (shown with one side clamp removed).**

The envelope geometry of each racetrack coil layer was also used to quantify the expected range in mass of each coil layer. This mass included the expected variation in the superconductor's density due to variations in the thickness and width of the conductor. The density variation was found to be very small for the 4 mm and 3 mm wide HTS used in the HEMM – 8923 kg/m$^3$ with a tolerance of -0.5 / +1 kg/m$^3$. This is a result of the very similar densities of Hastelloy C-276 (8890 kg/m$^3$) and copper (8930 kg/m$^3$). The calculated variation in coil layer mass should include any secondary constituents (epoxy, solder, current terminals, etc.) when those items can be predicted. The nominal mass of each coil layer is calculated from nominal dimensions and taken to be the average mass, $\mu_n$, of any coil layer $n$ that is produced. The standard deviation of the mass $\sigma_n$ is calculated from the tolerance range assuming the mass of manufactured coils follows a normal distribution where the high and low tolerances on the mass, $m_{n,\text{high}}$ and $m_{n,\text{low}}$, respectively, constitute the 99.7% confidence interval. Consequently, $\sigma_n = \left[\left(m_{n,\text{high}} - m_{n,\text{low}}\right)/2\right]/3$.

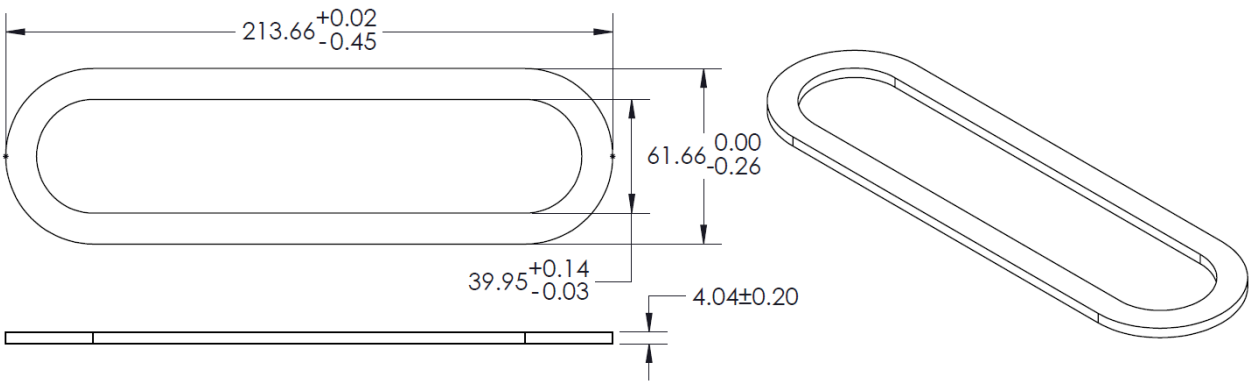


**Fig. 4 Envelope geometry of each of the HEMM's racetrack rotor coil layers according to a tolerance stack-up analysis of the machined and assembled winding fixture (dimensions in units of mm).**

For a rotor with $2p$ poles, there are $p$ coils that form north poles and $p$ coils that form south poles. The circumferential position of a north pole pancake coil for a given coil layer can be exchanged with that of any other north pole pancake coil from the same layer. The same is true for the south pole coil layers. Hence, there are $p!$ possible combinations of coil positions for each layer of the north poles and each layer of the south poles. A computer is used to randomly sample the mass of the $2p$ pancake coils for each of the $N$ coil layers from a normal distribution defined by the average and standard deviation noted above. The expected mass unbalance caused by the superconducting coils is calculated using one of two brute force methods. In method one, coils are randomly positioned on the rotor while satisfying the north/south pole and layer constraints. In method two, the coils are optimally positioned to minimize mass unbalance while satisfying the constraints. The unbalance of each coil is represented as a vector with magnitude equal to the mass of that rotor pole multiplied by the radius to the coil's center of mass, and then the overall unbalance is the vector sum of the individual unbalances, as depicted in Fig. 5. The optimal positioning was determined by first optimizing the circumferential position of each coil within a coil layer by calculating the unbalance for every possible set of positions and extracting the minimum unbalance of that layer. This was repeated for each coil layer. Next, the circumferential position of each layer relative to the other layers was optimized by calculating the total unbalance for every possible set of positions and extracting the minimum total unbalance. This process of sampling from a normal distribution, positioning coils and coil layers, and calculating the total unbalance is repeated thousands of times to produce a histogram of the total unbalance. A continuous distribution is fit to the histogram and then used to quantify the probability that the total unbalance will be below a certain value. A normal distribution was found to well represent the histograms obtained from approach one, but a log-normal distribution well represented the histograms in approach two.

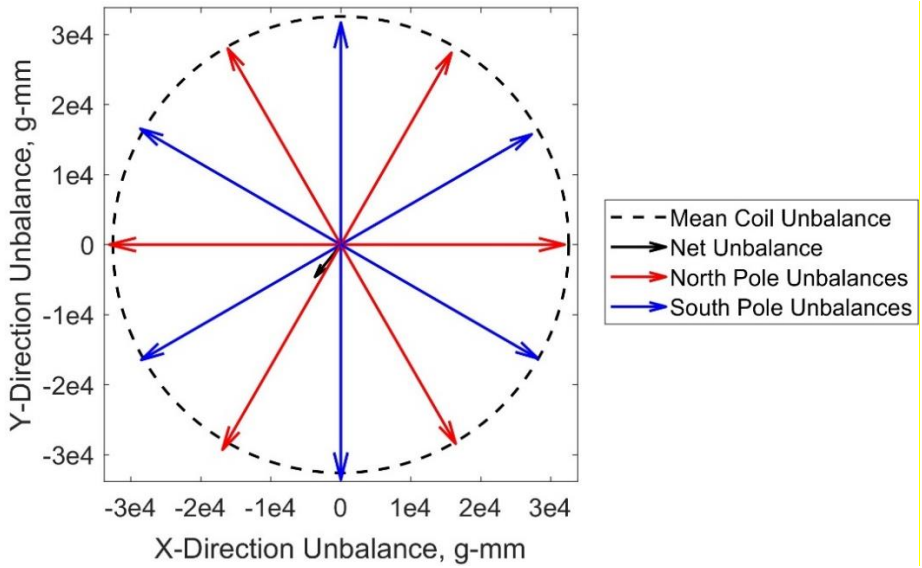


**Fig. 5 Example unbalance of a rotor with 12 poles due to the mass of superconducting coil layer 1.**

### A. Application to the HEMM

The coil mass variation calculated for each of the HEMM's rotor coil layers is summarized in Table 1. Note that coil layer 1 uses 4 mm wide HTS whereas the others use 3 mm wide HTS. Also note that the differences between coil layer 4 and layers 2 and 3 result from secondary constituents. 3,000 randomly sampled sets of twelve of each of the HEMM's four coil layers were used to evaluate the histograms for the two unbalance prediction methods. Fig. 6 depicts the histogram for method one (coils randomly positioned). A mean unbalance of about 4850 g-mm and a standard deviation of about 1,300 g-mm are observed when the histogram is fit with a normal distribution. Hence, there is predicted to be approximately a 95% chance that the total unbalance of the HEMM's rotor due to the superconducting coils is less than 6,990 g-mm when the coil layers are randomly positioned. This is equivalent to a 47 g mass at the outer diameter of the rotor. This is a considerably large mass correction that would necessitate the addition of design features for balancing via mass addition or mass removal.

**Table 1 Predicted tolerance on the mass (units of g) of each superconducting rotor coil layer for the HEMM.**

| Coil Layer | Nominal (average) | High Tolerance | Low Tolerance | Standard Deviation |
|---|---|---|---|---|
| 1 (largest radius) | 233 | 247 | 215 | 5.3 |
| 2 | 181 | 200 | 159 | 6.8 |
| 3 | 181 | 200 | 159 | 6.8 |
| 4 (smallest radius) | 202 | 214 | 187 | 4.5 |

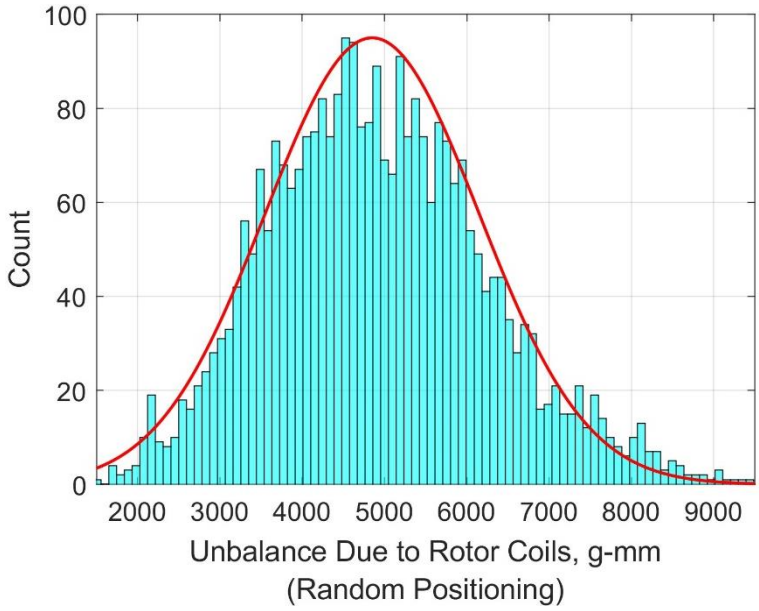


**Fig. 6 Histogram of total mass unbalance due to the HEMM's superconducting rotor coils when each coil layer is randomly positioned on the rotor (units of g-mm).**

The histogram for method two (coils optimally positioned) is shown in Fig. 7. The shape of the distribution is clearly different than for method one. In this case, a log-normal distribution with mean of about 3.25 and standard deviation of about 0.8 adequately fits the histogram. This indicates that there is approximately a 95% chance that the total unbalance of the HEMM's rotor due to the superconducting coils is less than 96 g-mm when the coil layers are optimally positioned. This is equivalent to a mass of only 0.6 g at the outer diameter of the rotor, which is a mass correction that can be readily accommodated.

For comparison, the ISO standard for unbalance indicates that the entire rotor should be balanced to G2.5, or 2.5 mm/s, at the maximum speed of 6,800 rpm. This is equivalent to 305 g-mm. This G2.5 specification applies to "electric motors and generators of at least 80 mm shaft height, of maximum rated speeds above 950 r/min." [10] Clearly,

optimizing coil mass distribution brings the unbalance level from unacceptably high (typically worse than G40) to well below the ISO standard.

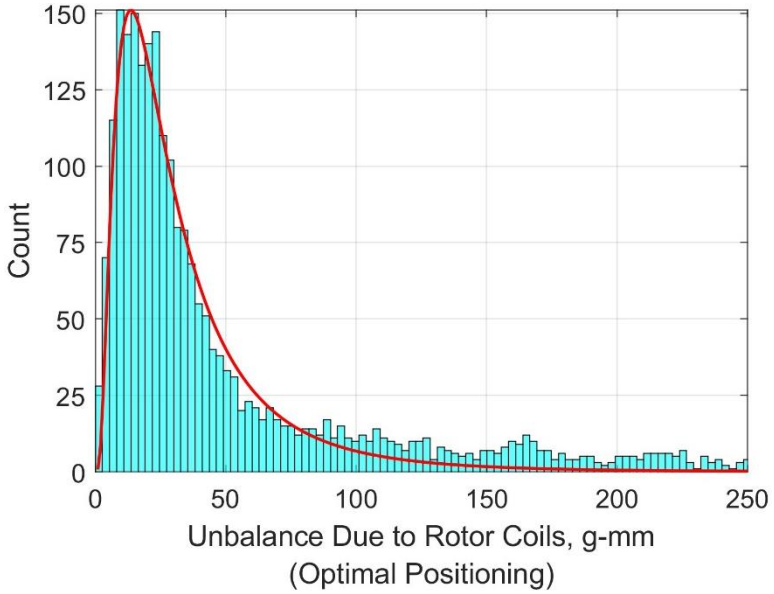


**Fig. 7 Histogram of total mass unbalance due to the HEMM's superconducting rotor coils when each coil layer is optimally positioned on the rotor to minimize unbalance (units of g-mm).**

It should be noted that the optimal positioning of coil layers can be easily accomplished by weighing each coil layer and determining the optimal positions before soldering the coil layers together to form rotor poles. Further, positioning the coil layers to minimize mass unbalance also positions the coils to best balance the number of turns in each coil, thereby balancing the magnetomotive force produced by each coil.

### B. Extension to Other Superconducting Machines

The unbalance expected in other superconducting machines depends on the geometric variation in each coil layer, which dictates the statistics of each layer's mass, and the number of rotor poles, which dictates the number of position combinations available. The HEMM has a relatively high number of poles for a superconducting machine. The analysis was repeated for a HEMM-like superconducting rotor that has 4 to 12 poles. Here, it is assumed that the statistics of the coil layer masses matches Table 1.

Figure 8 depicts the 95$^{th}$ percentile total unbalance for random and optimal coil positioning. Regardless of the number of rotor pole pairs, random positioning introduces more unbalance than optimal positioning, by a factor of 1.6 for 2 pole pairs and monotonically increasing to a factor of 73 for 6 pole pairs. The histograms for random and optimal positioning have similar forms to those in Figs. 6 and 7, respectively, except for 3 pole pairs, where the distribution that best fits the two positioning approaches is opposite. The results for 3 pole pairs also deviate from the general trend of unbalance increasing with number of pole pairs for random positioning and decreasing for optimal positioning.

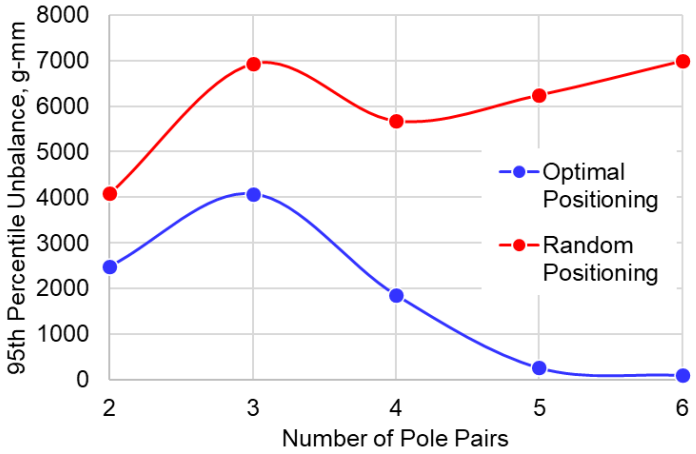


**Fig. 8 90th and 95th percentile total mass unbalance (units of g-mm) due to the randomly or optimally positioned coils on a HEMM-like superconducting rotor as a function of the number of rotor poles.**

## IV. Rotordynamics of the HEMM

### A. The HEMM geometry and rotordynamic requirements

Rotordynamics analysis is key to smooth operation of the HEMM, ensuring that any critical speeds are outside the operating speed range and that unbalance does not cause excessive displacements or bearing forces.

Figure 9 shows a cross section of the HEMM with its rotor and stator components. The rotor was conceived as having a cryocooler embedded within and rotating with the shaft. This cryocooler is comprised of a linear motor at the warm end (shown in green) that drives the acoustic pulses in the cryocooler (blue). The cold tip is closest to the rotor core, conductively cooling the rotor superconducting windings. The relatively large rotor shaft is supported within the stator on two sets of ball bearings. There is a single ball bearing (bearing 1) at the cold end near the rotor core and an angular contact pair (bearing 2) at the warm end near the linear motor. With this configuration, the rotor's center of mass will be outside the span of the ball bearings, meaning that the rotor core is overhung, requiring some kind of compliant bearing mount at the bearing 1 location. The design of this compliant mount will be key to ensuring any unbalance does not cause excessive radial displacements or bearing forces. The stator housing is mounted to the ground with three vibration isolation mounts in a single axial plane.

The magnetic interaction between the rotor and stator act like a negative stiffness between the two. It is far lower in magnitude than the stiffness of the bearings and mounts, but it does have an effect and was included in the analysis.

The rotor core and windings rotate inside a vacuum cylinder to eliminate losses due to drag. The rotor's maximum allowable radial displacement is determined by the gap between the rotor and the stator vacuum housing and the allowable radial motion at the vacuum seals.

Requirements for the HEMM motor's rotordynamics analysis are given in Table 2. The operating speed range is the idle speed through the operating speed, and critical speeds should be well away from that range. A critical speed is the rotor speed at which a rotor mode can be excited by unbalance, where the excitation frequency is equal to the rotor speed. The criteria for critical speeds are

- rigid body critical speeds should allow a 15% speed margin on any steady state operating speeds; and
- bending mode critical speeds should be at least 15% above the maximum operating speed.

The allowable radial displacement of the rotor relative to the stator is dictated by the gap between the rotor core and vacuum tube, as well as any seal specifications. One proposed seal that would be located near bearing 1 allows for radial eccentricities as high as 0.23 mm at maximum speed (higher at lower speeds) and a non-concentric position relative to the shaft operating centerline of 0.25 mm radial. Therefore, the rotor static and dynamic displacements relative to the stator need to add to less than those values together at that location.

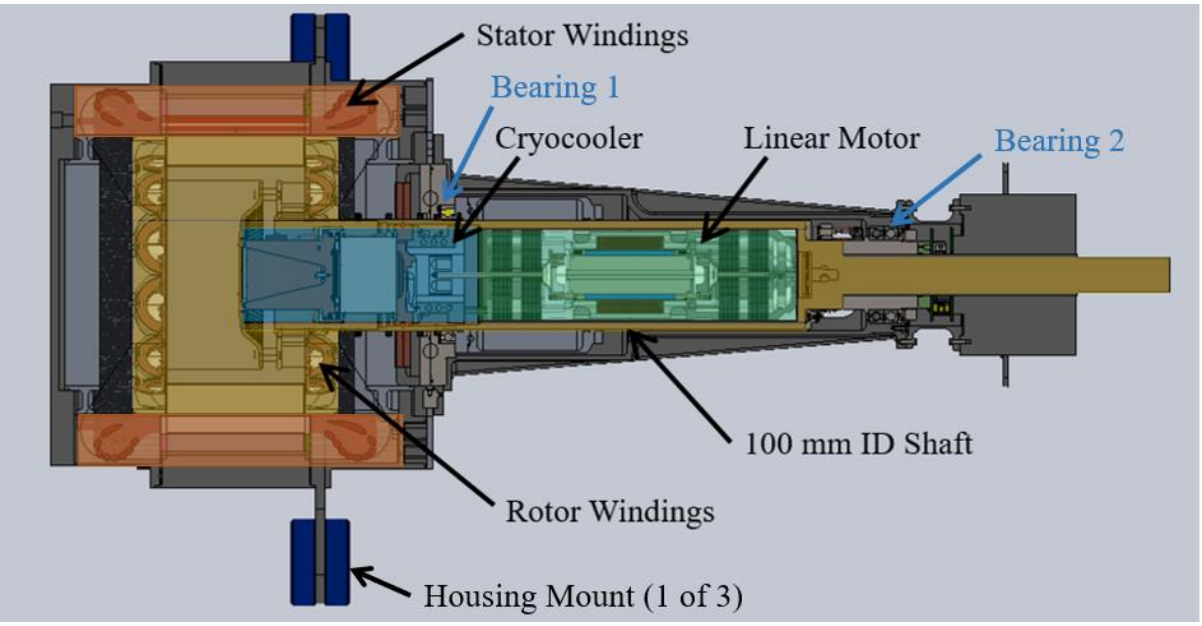


**Fig. 9 The HEMM motor configuration showing bearings and housing mount locations.**

**Table 2 The HEMM rotordynamic requirements.**

| Parameter | Value |
|---|---|
| Operating Speed | 6,800 rpm |
| Idle Speed (assumed 60% of operating speed) | 4,080 rpm |
| Maximum operating speed (assumed 105%) | 7,140 rpm |
| Gap between rotor core and vacuum housing | 1.0 mm radial |
| Rotor mass | 86.8 kg |
| Bearing 1 dynamic load rating | 78 kN |
| Bearing 2 dynamic load rating (bearing pair) | 35.8 kN each/71.6kN both |
| Vacuum seal allowable non-concentric position | 0.25 mm |
| Vacuum seal allowable radial eccentricity at max speed | 0.23 mm |
| Rigid body modes | < 3,468 rpm<br>> 7,820 rpm |
| Bending modes | > 8,211 rpm |

One thing to note is that the linear motor located within the shaft is designed to be oscillating axially at approximately 60 Hz, or 3,600 rpm, and it would be best to keep any resonance modes away from that frequency.

The rotordynamic analysis was performed using two methods: a full finite element analysis and a spreadsheet-based rotordynamics code. In both cases, the structural elements providing stiffness to the rotor are included directly, and other elements (e.g. superconducting coils, integrated cryocooler) are included as added mass and inertia. The spreadsheet-based code requires radial and angular stiffnesses between the rotor core and shaft representing the torque

web (torque-transfer connection part) and thermal bridge (thermal-transfer connection part). Those values were determined through finite element analysis, matching mode frequencies and mode shapes.

**B. Rotordynamics analysis**

Since the HEMM's rotor is overhung, with the center of mass to the left of both bearings as shown in Fig. 9, there was some concern that the rotor's radial displacements could be very large during operation. A typical way to deal with an overhung rotor is to incorporate a well-damped compliant mount at the bearing location closest to the center of mass, in this case bearing 1. To guide the design of the compliant mount, a critical speed analysis was done for the rotor alone, varying the stiffness value $K_1$ for bearing 1 and assuming bearing 2 has a stiffness of $K_2 = 1.0 \times 10^5$ N/mm to account for the ball bearing's stiffness and the inherent housing stiffness of bearing 2. The stiffness of bearing 1 was varied from $1 \times 10^4$ N/mm (soft mount) to $1 \times 10^5$ N/m (hard mount). The negative stiffness was set at -1724 N/mm applied at the axial center of the rotor core.

The critical speed map is given in Fig. 10, showing how the first two critical speeds change with the stiffness of bearing 1. A forward whirl mode can be excited by unbalance since its motion is in the same circumferential direction as unbalance. Backward whirl modes have motion in the opposite direction and cannot be excited by unbalance. As $K_1$ increases from the soft mount to the hard mount values, the first mode increases and enters the keep-out speed range of 3,468-7,820 rpm for rigid body modes.

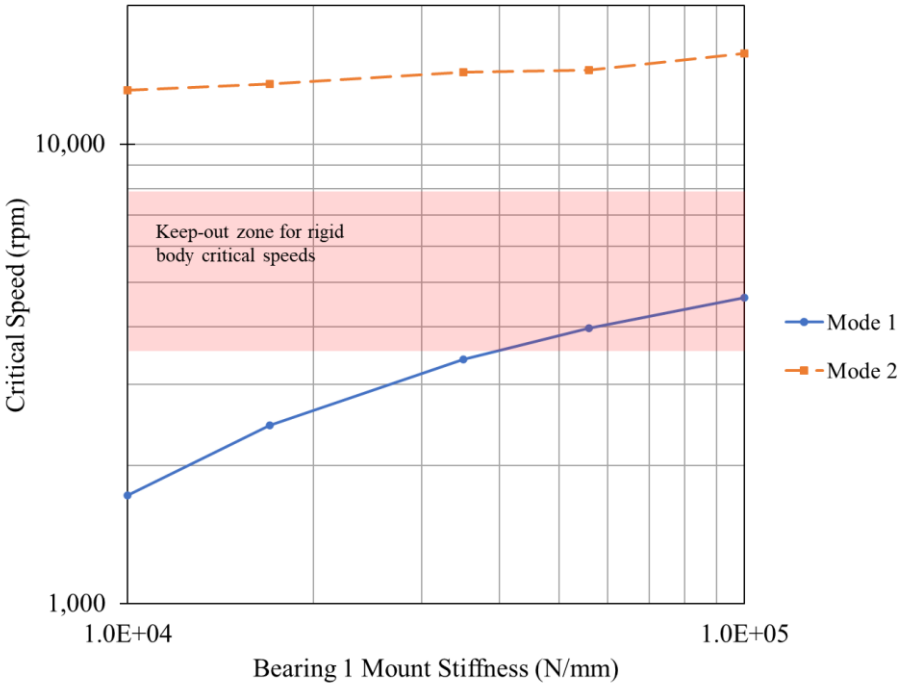


**Fig. 10 Critical speed map for varying the stiffness of bearing 1, with $K_2 = 1 \times 10^5$ N/mm.**

Figure 11 depicts the first two mode shapes for $K_1 = 3.5 \times 10^4$ N/mm, the highest allowable stiffness for the critical speed to remain just below the keep-out speed range. It can be seen that for mode 1 the maximum displacement is at the rotor core, justifying the concern for rotor core displacement during operation.

Figure 12 shows the Campbell diagram for $K_1 = 3.5 \times 10^4$ N/mm. Note that at 6,800 rpm, the forward whirl frequencies for modes 2 and 3 are 220 Hz and 290 Hz respectively, which are 94% and 156% above the 113 Hz unbalance excitation frequency.

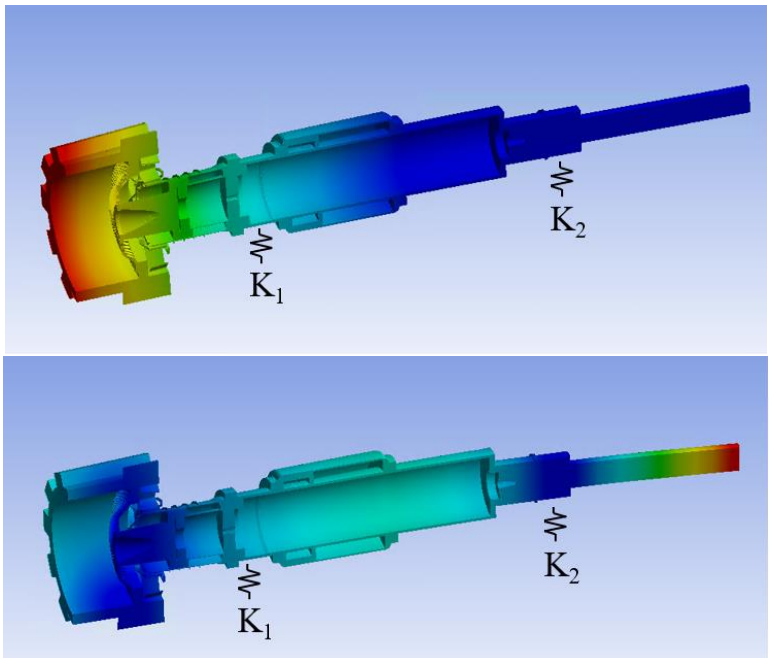


**Fig. 11 Rotordynamic mode 1 (top) and mode 2 (bottom) for $K_1$ = 3.5x10$^4$ N/mm and $K_2$ = 1x10$^5$ N/mm, blue is zero displacement, red is maximum displacement.**

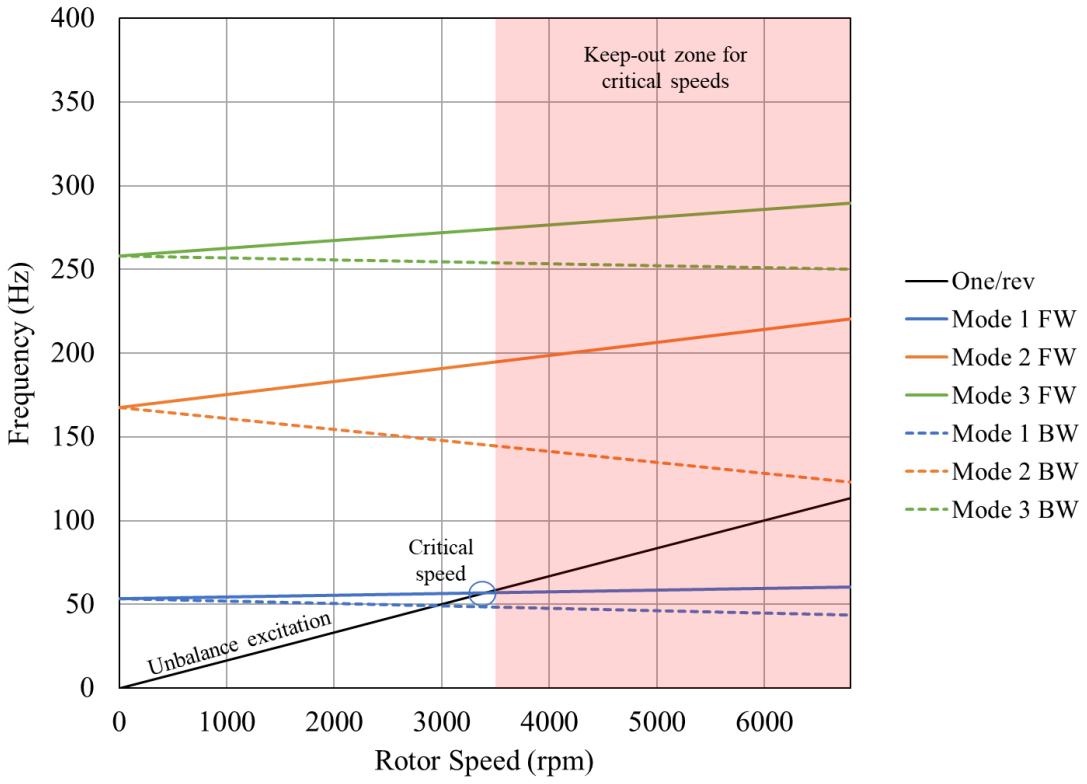


**Fig. 12 Campbell diagram for $K_1$ = 3.5x10$^4$ N/mm, FW = forward whirl, BW = backward whirl.**

An aircraft-installed motor will experience various loading scenarios during flight, which will affect the choice of bearing mount stiffness. However, this iteration of the motor design is intended to be tested on the ground. Since the rotor orientation will be horizontal, a soft bearing will cause the rotor to sag due to gravity. Recall that the proposed seal near bearing 1 allows for radial eccentricities as high as 0.23 mm at maximum speed and a non-concentric position relative to the shaft operating centerline of 0.25 mm radial. Therefore, the rotor static and dynamic displacements at the seal need to add to less than those values together, or 0.48 mm. It was decided to target a sag due to gravity of less than 0.1 mm, to allow for higher dynamic displacement. Figure 13 shows the sag due to gravity as a function of bearing 1 stiffness. A stiffness of at least $2x10^4$ N/mm would accomplish that goal.

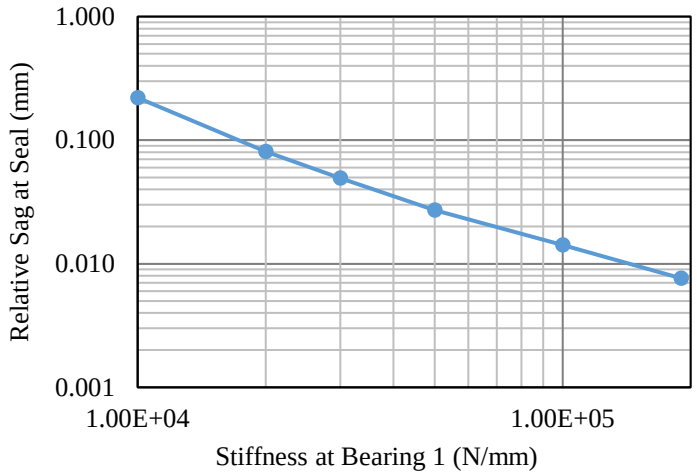


**Fig. 13 Relative sag at seal location as a function of $K_1$ when $K_2$ = $1x10^5$ N/mm.**

One thing to note is that unbalance force is proportional to the square of the rotor speed. Figure 14 shows the unbalance amount as a function of rotor speed, for two different levels of unbalance, G2.5 (2.5 mm/s at maximum operating speed, which is the correct specification for this motor) and G6.3 (6.3 mm/s which applies to smaller motors and is more conservative). Keeping the critical speeds low means that unbalance force at the critical speed will be lower, and thus the rotor's response will be lower.

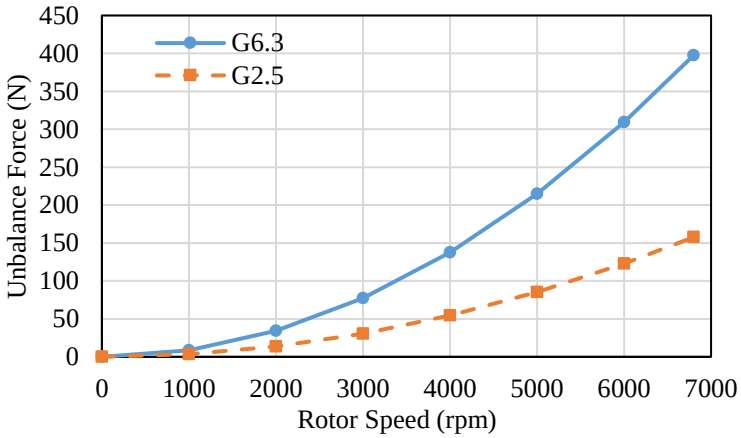


**Fig. 14 Unbalance force versus rotor speed and unbalance level.**

The next analysis calculated radial displacements and bearing forces due to unbalance. To be conservative, the higher G6.3 unbalance level was used as well as a stiffness of $K_1 = 3.5x10^4$ N/mm to give the highest allowable critical speed for the operating speed range. These calculations were done with a loss factor $\eta$ of 0.1, assumed constant over the speed range. The damping C is then defined by $C = K\eta/\omega$, where $\omega$ is the angular frequency of oscillation. Figure 15 shows results for the rotor displacement at the end of the rotor core for the higher G6.3 unbalance level, and Fig.

16 displays the radial displacement at locations along the rotor at the critical speed. This analysis was done using both FEA and with a spreadsheet-based rotordynamics code. Analysis was done for the rotor alone and also including the stator with vibration isolation mounts to verify the validity of the rotor-alone analysis.

The seal's axial location is roughly 200 mm in Fig. 16, which gives a resonant displacement of about 0.12 mm. The sum of the sag and the dynamic response total to 0.16 mm, well below the seal allowable of 0.48 mm. The free end of the rotor core has a displacement of less than 0.25 mm, well below the rotor/vacuum cylinder gap of 1.0 mm. Finally, the resonant forces on the bearings are less than 1000 lb, well below the dynamic load ratings of the bearings, though the steady force on the bearings should be used to calculate bearing life.

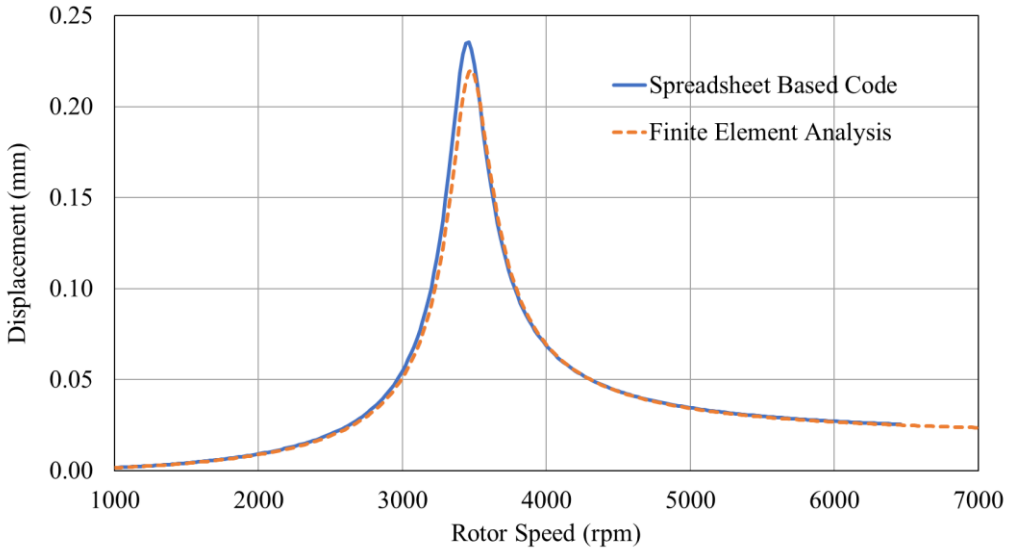


**Fig. 15 Unbalance response at 'free' end of rotor core (largest radial displacement location).**

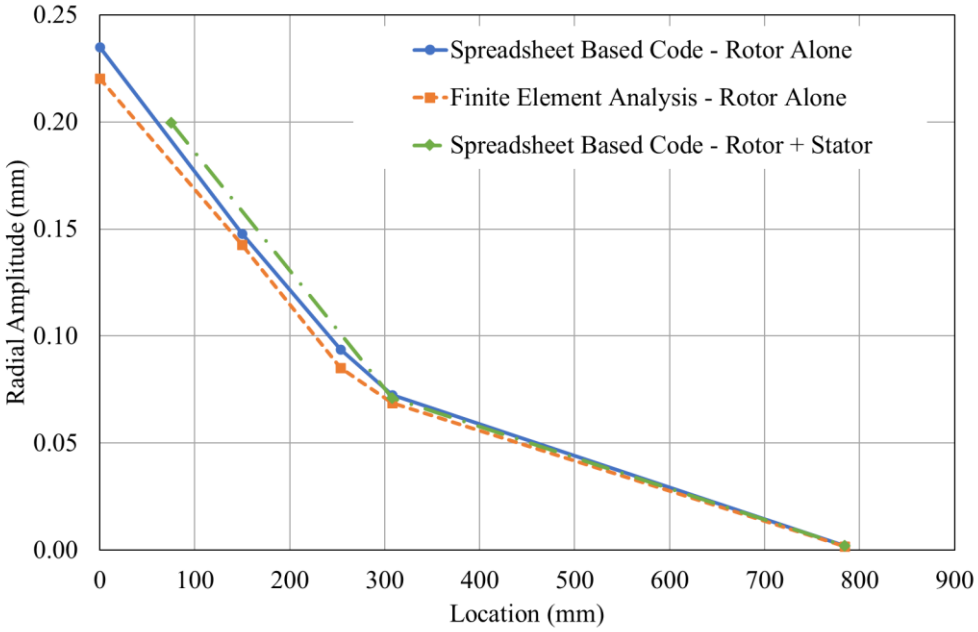


**Fig. 16 Radial displacement at critical speed of 3450 rpm versus axial location on rotor.**

Note that the resonant frequency of 3,450 rpm is near the linear motor design frequency of 60 Hz, with only 4% margin. Care must be taken to give sufficient margin to the linear motor frequency, so a mount stiffness less than $K_1 = 3.5x10^4$ N/mm will be required. The lower critical speed will yield lower unbalance force at resonance, which will in turn decrease rotor displacement and bearing force levels.

### C. Discussion

The remaining challenge is how to provide the desired stiffness and damping at the bearing 1 location. A complication for the design is that there is limited space available, due to the cryocooler's cooling system being located in the vicinity. Three types of compliant mounts have been investigated: a squeeze film damper (SFD), a metal mesh support, and an elastomeric support. The SFD could use the existing cooling fluid but would require a centering spring that needs more radial or axial space than is optimal. Metal mesh supports or elastomeric supports can be implemented in a more compact form than the squeeze film damper; however, both have nonlinear stiffness and damping characteristics, and would require material and component testing to design final configurations. Preliminary calculations show that any of these concepts can provide the necessary stiffness and damping to keep the HEMM operation smooth and stable. Next steps will be to build and test the compliant mount hardware.

Based on the experience of specifying the bearing mount properties for the HEMM overhung rotor, as well as with building and testing the linear motor [9], it is expected that future iterations of motor design will include two opposing cryocoolers. This will allow for a more standard rotor shaft mounting design, with the center of mass between the bearings, simplifying the design for rotordynamics. In addition, the opposing linear motor forces will cancel each other, producing a much smaller oscillating axial force and reducing potential vibration problems. That configuration may also allow for vacuum seals with more favorable radial displacement allowances, since the large surface speed of the current seal narrowed the available options significantly.

## V. Conclusion

In this study, the potential unbalance arising from the fabrication and installation of superconducting rotor coils is studied, with particular note of the impact of imprecise winding lengths and tolerance stack up during winding. A method was introduced to predict and minimize this unbalance, to keep the level well within acceptable standards for the HEMM motor in particular. This technique can be implemented for any motor with rotor windings. With the unbalance level predicted, a rotordynamics analysis was performed, with emphasis on dealing with the overhung nature of the rotor. The bearing mount closest to the center of mass dictates the first critical speed, which must be placed below the operating speed range (idle speed to maximum operating speed). The second critical speed remains well above the operating speed range. Levels of stiffness and acceptable damping were determined for this bearing mount for a conservative unbalance level. The bearing mount must now be designed with guidance from the rotordynamics analysis.

## Acknowledgments

This work was supported by the NASA Advanced Air Transportation Technologies Project – Aircraft Electrification Subproject managed by Amy Jankovsky within NASA's Aeronautics Research Mission Directorate.

## References

[1] Brown, G. V., "Weights and Efficiencies of Electric Components of a Turboelectric Aircraft Propulsion System," *Proceedings of the 49th AIAA Aerospace Sciences Meeting*, Orlando, FL, 2011. doi: 10.2514/6.2011-225

[2] Schnulo, S. L. et al., "Assessment of the Impact of an Advanced Power System on a Turboelectric Single-Aisle Concept Aircraft," *Proceedings of the 2020 AIAA/IEEE Electric Aircraft Technologies Symposium (EATS)*, New Orleans, LA, 2020. doi: 10.2514/6.2020-3548

[3] J. R. Welstead and J. L. Felder, "Conceptual Design of a Single-Aisle Turboelectric Commercial Transport with Fuselage Boundary Layer Ingestion," *Proceedings of the AIAA SciTech 2016 Forum*, San Diego, 2016. doi: 10.2514/6.2016-1027

[4] Szpak, G. et al., "High Efficiency Megawatt Motor Thermal Stator Preliminary Design," *Proceedings of the 2020 AIAA/IEEE Electric Aircraft Technologies Symposium (EATS)*, New Orleans, LA, 2020. doi: 10.2514/6.2020-3602

[5] Jansen, R.H. et al., "High Efficiency Megawatt Motor Preliminary Design," *Proceedings of the 2019 AIAA/IEEE Electric Aircraft Technologies Symposium (EATS)*, Indianapolis, IN, 2019.
doi: 10.2514/6.2019-4513
[6] Tallerico, T.F., "Electromagnetic Redesign of NASA's High Efficiency Megawatt Motor," *Proceedings of the 2020 AIAA/IEEE Electric Aircraft Technologies Symposium (EATS)*, New Orleans, LA, 2020.
doi: 10.2514/6.2020-3600
[7] Scheidler, J.J. et al., "Progress Toward the Critical Design of the Superconducting Rotor for NASA's 1.4 MW High-Efficiency Electric Machine," *Proceedings of the 2019 AIAA/IEEE Electric Aircraft Technologies Symposium (EATS)*, Indianapolis, IN, 2019.
doi: 10.2514/6.2019-4496
[8] Dyson, R.W. et al., "High Efficiency Megawatt Machine Rotating Cryocooler Conceptual Design," *Proceedings of the 2019 AIAA/IEEE Electric Aircraft Technologies Symposium (EATS)*, Indianapolis, IN, 2019.
doi: 10.2514/6.2019-4515
[9] Duffy, K.P. et al., "Design, Analysis, and Testing of the HEMM Cryocooler Linear Motor," *Proceedings of the 2020 AIAA/IEEE Electric Aircraft Technologies Symposium (EATS)*, New Orleans, LA, 2020.
doi: 10.2514/6.2020-3601
[10] International Standard ISO 1940-1:2003(E), "Mechanical vibration – Balance quality requirements for rotors in a constant (rigid) state – Part 1: Specification and verification of balance tolerances."